Transformer-Flux-Balancing Control in Isolated Bidirectional Dc-Dc Converters

Yuri Panov, Milan M. Jovanović, Liu Gang, and Meng Yueyong
Delta Products Corporation
P.O. Box 12173
5101 Davis Drive
Research Triangle Park, NC 27709, USA

***Abstract* - The paper presents novel transformer-flux-balancing control methods for the isolated bidirectional full-bridge (FB) converter with active clamp and the bidirectional dual-active bridge (DAB) converter. Both approaches are based on the sensing and control of the transformer magnetizing current. For the isolated bidirectional FB converter the magnetizing current is obtained by sensing a single current, whereas for the DAB converter, both primary and secondary currents of the transformer need to be sensed to obtain the magnetizing current. Since in the DAB converter the magnetizing-current control can lead to excessive dc values of the winding currents, an additional control loop that eliminates the dc value of the primary and secondary currents is introduced. Performance of the proposed flux-balancing control for the isolated bidirectional FB converter was experimentally evaluated on a 2-kW prototype.**

I. Introduction

Today, bidirectional converters are increasingly finding applications in power systems with energy-storage capability, most notably in "smart"-grid and automotive applications [1]. Generally, they are employed to condition charging and discharging of the energy-storage devices such as batteries and supercapacitors. Specifically, in automotive applications, isolated bidirectional dc-dc converters are used in electric vehicles (EVs) to provide bidirectional energy exchange between the high-voltage (HV) and low-voltage (LV) battery, whereas bidirectional ac-dc converters are required for future vehicle-to-grid (V2G) applications. Due to a relatively wide battery-voltage range that is dependent on battery's state of charge, achieving high efficiency across the entire battery voltage range is a major design challenge of bidirectional dc-dc converters.

Two most widely used bidirectional isolated converter topologies are the full-bridge (FB) converter with active clamp [2] and the dual-active-bridge (DAB) converter [3], shown in Figs. 1(a) and (b), respectively. Various aspects of their performance optimization are addressed in numerous papers. The majority of these papers are focused on their efficiency improvements through power-stage refinements and advanced control techniques [4]-[9].

However, the transformer saturation issue, which is of the paramount importance for reliable operation of isolated bidirectional converters, is almost completely ignored in the literature, although isolated bidirectional converters may be more susceptible to the transformer saturation than their unidirectional counterparts. Namely, because in bidirectional converters both the primary and secondary side of the transformer are connected to voltage sources, any differences of duty cycles caused by mismatching of drive signals timing and/or unequal voltage drops on semiconductor switches cause a difference in positive and

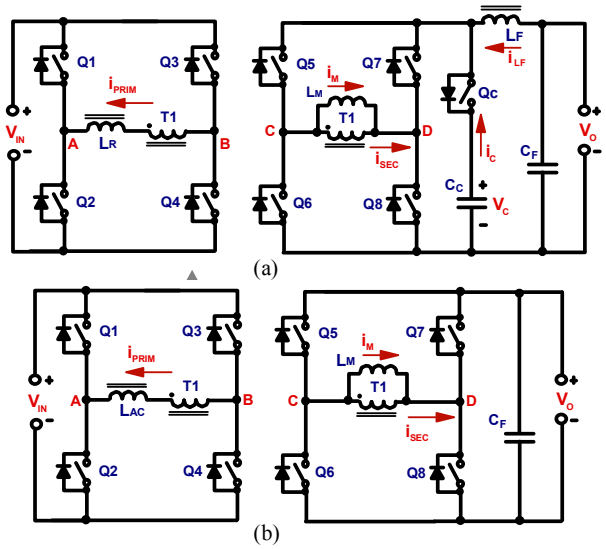

Fig.1. Two isolated bidirectional topologies: (a) FB converter with active clamp; (b) DAB converter.

negative volt-seconds, which leads to flux walking that eventually may result in transformer core saturation. Except for reference [10] that addresses the transformer design to avoid saturation in DAB converter, no other literature deals with this design aspect of bidirectional converters.

Generally, passive and active approaches used in unidirectional isolated FB converters to eliminate transformer saturation due to flux walking can also be applied in bidirectional converters. Passive approaches include conservative transformer designs with a low peak flux density and large core gap that can absorb the anticipated worst-case flux imbalance without saturating the core [10]-[11] and adding blocking capacitors in series with the primary and/or secondary winding of the transformer to eliminate their dc currents [12]. These passive approaches are not desirable because the transformer overdesign approach requires an increased peak value of the magnetizing current which increases conduction and switching losses, whereas the blocking-capacitor approach requires additional components that increase the size and cost.

A number of active approaches that are based on sensing of transformer currents and using sensed signals to modify duration of driving signals of the switches to maintain flux balance in unidirectional isolated FB converters have been introduced in [13]-[15]. In most applications, sensing of only primary current is

978-1-4799-2325-0/14/$31.00 ©2014 IEEE

sufficient for the flux-balancing control [13]-[14]. However, in some applications, such as plasma-cutting power supplies, sensing of the transformer magnetizing current is required which is achieved by sensing both primary and secondary currents [15].

In this paper, a novel flux-balancing method for the isolated FB bidirectional converter based on direct control of the magnetizing current is proposed. In the proposed method, the peak value of the magnetizing current is obtained by sensing a single current waveform. In addition, the paper introduces a flux-balancing control of the DAB converter that is also based on the magnetizing current control. In this control, sensing of both primary and secondary currents is required. Since in DAB converter the magnetizing-current control can lead to the excessive dc values of the winding currents, an additional control loop that reduces the dc values of the primary and secondary currents down to zero is introduced.

The paper is organized in five sections. Principles of the active flux-balancing control, applicable to unidirectional and bidirectional converters, are discussed in Section II. Section III presents the proposed single-current-sensing flux-balancing control of the isolated FB bidirectional converter, whereas Section IV presents the proposed two-loop flux-balancing control of the DAB converter. Summary and future work are presented in Section V.

II. Principles of Active Flux-Balancing Control

The analysis of the isolated FB bidirectional converter in Fig. 1(a) and DAB converter in Fig. 1(b) can be facilitated by recognizing that during time periods when active-clamp switch Q_C in Fig. 1(a) is closed, the equivalent circuit of the isolated FB bidirectional converter is the same as that of the DAB converter. In this common equivalent circuit shown in Fig. 2, voltage source $\mathbf{V_{EQ}}$ is equal to voltage $\mathbf{V_C}$ of clamp capacitor C_C for the isolated FB bidirectional converter and to voltage V_O for the DAB converter. Equivalent inductance L_{EQ} in Fig. 2 can be an external inductance or the transformer leakage inductance, or their sum.

Generally, since the flux in the transformer core cannot be sensed directly, the active flux-balancing control is based on the magnetizing current control because magnetizing current $\boldsymbol{i_M}$ is related to flux $\boldsymbol{\Phi}$ as

$$\boldsymbol{L_M \cdot i_M = N_S \cdot \Phi} \qquad (1)$$

where $\boldsymbol{L_M}$ and $\boldsymbol{N_S}$ are secondary-side magnetizing inductance and number of secondary turns, respectively. Because according to Ampere's law, magnetizing current $\boldsymbol{i_M}$ is the difference between secondary and reflected primary current, i.e.,

$$\boldsymbol{i_M = i_{SEC} - N_P/N_S \cdot i_{PRIM}}, \qquad (2)$$

it can be calculated by measuring secondary current $\boldsymbol{i_{SEC}}$ and primary current $\boldsymbol{i_{PRIM}}$ and knowing transformer turns ratio $\boldsymbol{N_P/N_S}$.

Waveforms of secondary-winding voltage $\boldsymbol{V_{CD}}$ and magnetizing current $\mathbf{i_M}$, that has a positive dc bias, are shown in Fig. 3. Magnitudes of $\boldsymbol{V_{CD}}$ positive and negative pulses are $\boldsymbol{V_{EQ(P)}}$ and $\boldsymbol{V_{EQ(N)}}$, respectively, which are not equal due to mismatching of the voltage drops on conducting switches. The goal of the flux-balancing control is to maintain dc component $\boldsymbol{i_M^{dc}}$ of the magnetizing current and, therefore, the dc component of flux $\boldsymbol{\Phi}$ well below the saturation level by adjusting the on-times of positive and negative $\boldsymbol{V_{CD}}$ pulses, i.e., by adjusting the volt-second product across the transformer winding. As illustrated in Fig. 3, for the magnetizing current which has a positive dc bias during

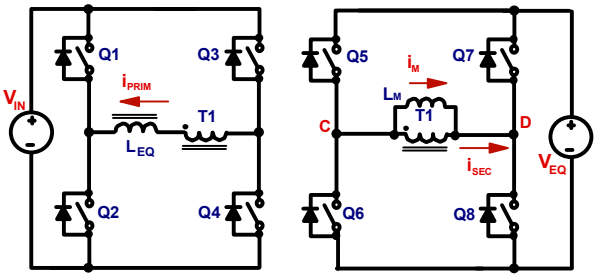

Fig. 2. Common equivalent circuit of both bidirectional topologies.

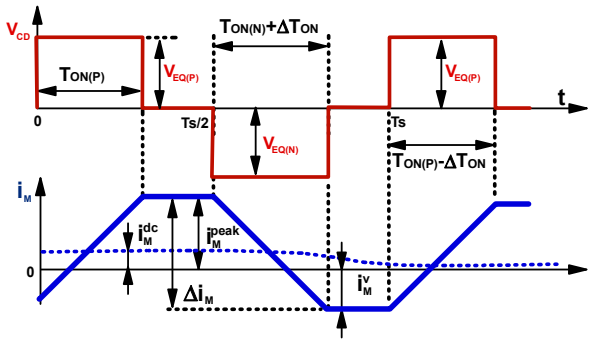

Fig. 3. Waveforms of secondary voltage V_{CD} and magnetizing current i_M with positive dc bias.

time interval $\boldsymbol{0 \le t \le T_S/2}$, the control needs to increase on-time $\boldsymbol{T_{ON(N)}}$ of $\boldsymbol{V_{CD}}$ negative pulse by $\boldsymbol{\Delta T_{ON}}$ and/or decrease on-time $\boldsymbol{T_{ON(P)}}$ of $\boldsymbol{V_{CD}}$ next positive pulse by $\boldsymbol{\Delta T_{ON}}$.

The steady-state peak-to-peak value of magnetizing current $\boldsymbol{\Delta i_M}$ is determined by

$$\boldsymbol{\Delta i_M = \left(V_{EQ}/L_M\right) \cdot T_{ON} = \left(V_{EQ}/L_M\right) \cdot \left(d \cdot T_S/2\right)}, \qquad (3)$$

where $\boldsymbol{T_S}$ and $\boldsymbol{d}$ are the switching period and the steady-state secondary-side duty ratio, respectively. Generally, condition for avoiding transformer saturation is

$$\boldsymbol{i_M^{dc} + \Delta i_M/2 < N_S \cdot B_{SAT} \cdot A_C/L_M}\ , \qquad (4)$$

where $\boldsymbol{B_{SAT}}$ and $\boldsymbol{A_C}$ are the transformer core saturation flux density and cross-sectional area, respectively. From Eqs. (3) and (4), maximum magnetizing current dc value $\boldsymbol{i_{M\,(max)}^{dc}}$ which brings the core flux density to the saturation level is

$$\boldsymbol{i_{M\,(max)}^{dc} = \left(N_S \cdot B_{SAT} \cdot A_C - \frac{1}{4} \cdot V_{EQ} \cdot d_S \cdot T_S\right)/L_M}\ . \qquad (5)$$

A flux-balancing control must keep the dc level of the magnetizing current below the maximum value defined by (5) with an ample margin. In fact, for optimal design of the transformer, it is desirable to completely eliminate the dc component of the magnetizing current, i.e., to make it zero.

Sensing of dc component $\boldsymbol{i_M^{dc}}$ that is required to implement the proposed control can be done in two ways. One approach is to measure and equalize the absolute values of peak $\boldsymbol{i_M^{peak}}$ and valley $\boldsymbol{i_M^{v}}$ levels of the magnetizing current. The other approach is to measure the dc bias directly by measuring magnetizing current at the middle of the secondary voltage on-time, i.e., at time instants $\boldsymbol{T_{ON(P)}/2}$ or $\boldsymbol{T_S/2 + \left(T_{ON(N)} + \Delta T_{ON}\right)/2}$, and adjust the on-times to keep this value to approximately zero. The latter approach

is better suited for digital implementation of flux-balancing control. With this approach, single sampling of the magnetizing current per switching period is sufficient for the control.

III. Flux-Balancing Control Of FB Bidirectional Converter

For the isolated FB bidirectional converter in Fig. 1(a), the transformer flux-balancing control is implemented differently during the buck and boost modes. In the buck mode, when energy flows from source V_{IN} to V_O, flux balancing is achieved by using the traditional peak-current-mode control with primary-current sensing.

To facilitate the explanation of the flux-balancing control in the boost mode, key waveforms for this mode are shown in Fig. 4. In the boost mode, primary-side devices Q1-Q4 are turned off and primary current flows through their antiparallel diodes, i.e., the primary side works as a full-bridge rectifier. As it can be seen from Fig. 4, during switching cycle $t_1 \le t \le t_7$, primary current i_{PRIM} is zero during time intervals $t_3 \le t \le t_4$ and $t_6 \le t \le t_7$. As a result, during these intervals, secondary current i_{SEC} is equal to magnetizing current i_M. Therefore, sensing of the secondary current during $t_3 \le t \le t_4$ and $t_6 \le t \le t_7$ is equivalent to sensing peak i_M^{peak} and valley i_M^v values of the magnetizing current, respectively. It should be noted that during time intervals $t_3 \le t \le t_4$ and $t_6 \le t \le t_7$, clamp switch Q_C is off while switches Q5-Q8 are on, i.e., the secondary winding of the transformer is shorted.

The block diagram of the analog implementation of the flux-balancing control based on the proposed sensing of the magnetizing current and its key waveforms are shown in Figs. 5(a) and (b), respectively. As shown in Fig. 5(a), the secondary current is sensed by the sensor with gain R_S and rectified by the full-wave rectifier. The amplified rectified sensed signal is then added to the PWM ramp during the time intervals when the primary current is zero, i.e., when the sensed current is equal to the magnetizing current, by closing switch S1. As illustrated in Fig. 5(b), during time intervals when the primary current is zero, output signal d_S of the PWM comparator is high. However, the turn-on instant of switch S1 in Fig. 5(a) is delayed for time T_D with respect to the rising edge of signal d_S to allow the primary current to decrease from its peak value to zero during time intervals $t_2 \le t \le t_3$ and $t_5 \le t \le t_6$, as shown in Fig. 4. As a result, signal V_{SUM} at the inverting input of the PWM comparator appears as shown in Fig. 5(b). Duty cycles d_1 and d_2 are adjusted in the direction which reduces imbalance between i_M^{peak} and i_M^v absolute values so that the dc component of the magnetizing current is minimized. It will be shown in the next subsection that proportional control is sufficient to obtain fast, stable, and reasonably accurate regulation of the dc component of the magnetizing current.

(A) Analysis of Flux-Balancing Control

The following analysis of the flux-balancing control is based on the discrete-time model which relates magnetizing current values at adjacent switching periods.

As can be seen from Fig. 5(a), without flux-balancing control, i.e., when switch S1 is open, the duty ratio at the output of the PWM comparator is given by

$$D = V_{EA}/V_{RAMP}$$

where V_{EA} is the error amplifier output voltage and V_{RAMP} is the peak-to-peak magnitude of the PWM ramp. This duty ratio at the

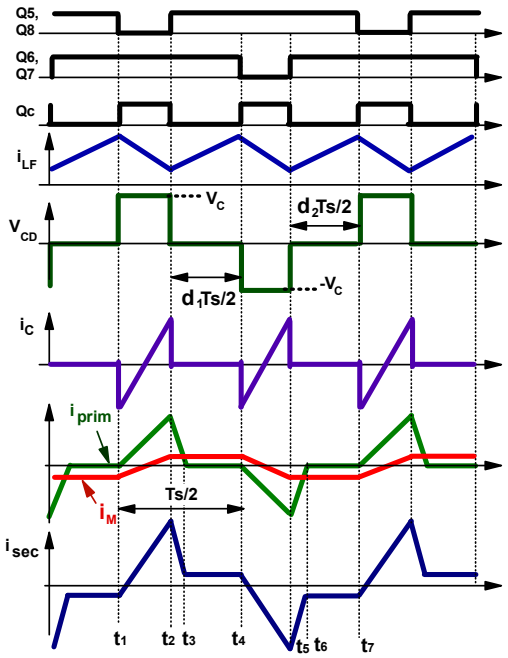

Fig. 4. Key waveforms of FB bidirectional converter in boost mode.

output of the PWM comparator is the same for both positive and negative secondary voltage V_{CD}. However, due to differences in the power device switching times and propagation delays of their driving circuits, the actual duty ratios applied to the transformer winding during positive and negative voltage V_{CD} may be different. Assuming that without flux-balancing control positive and negative pulses of voltage V_{CD} have on-times $T_{ON(P)}$ and $T_{ON(N)}$, respectively, and $T_{ON(P)} \ne T_{ON(N)}$, the on-times are related to duty cycle D of PWM output signal d_S as

$$T_{ON(P)} = (1 - D) \cdot T_S/2, \quad (7)$$

$$T_{ON(N)} = (1 - D - \Delta d) \cdot T_S/2, \quad (8)$$

where Δd is the duty ratio imbalance caused by the difference of the on-times, i.e.,

$$\Delta d = \left(T_{ON(P)} - T_{ON(N)}\right)/(T_S/2). \quad (9)$$

To model the effect of unbalanced magnitudes of the positive and negative V_{CD} voltages during adjacent half cycles, the values of the secondary voltage during the first and second half-cycles of the same cycle are considered to be V_{CP} and V_{CN}, respectively, and $V_{CP} \ne V_{CN}$. It should be noted that the worst-case volt-second imbalance occurs when the voltage difference $(V_{CP} - V_{CN})$ and duty-ratio difference given by Eq. (9) have the same sign because in that case the difference in positive (setting) and negative (resetting) volt-seconds is maximal. For example, if $T_{ON(P)} > T_{ON(N)}$, then the worst-case voltage-second imbalance occurs for $V_{CP} > V_{CN}$.

With flux-balancing control applied, inspection of Fig. 5 shows that during the first half of the k-th switching cycle, magnetizing current i_M, voltage V_{EA}, and PWM ramp signal are related as

$$d_1[k] \cdot V_{RAMP} + R_S \cdot K_1 \cdot |i_M^V[k]| = V_{EA}, \quad (11)$$

To facilitate further analysis, it is assumed that $i_M^V[k] < 0$ and $i_M^{peak}[k] > 0$. It is also assumed that the flux-balancing control

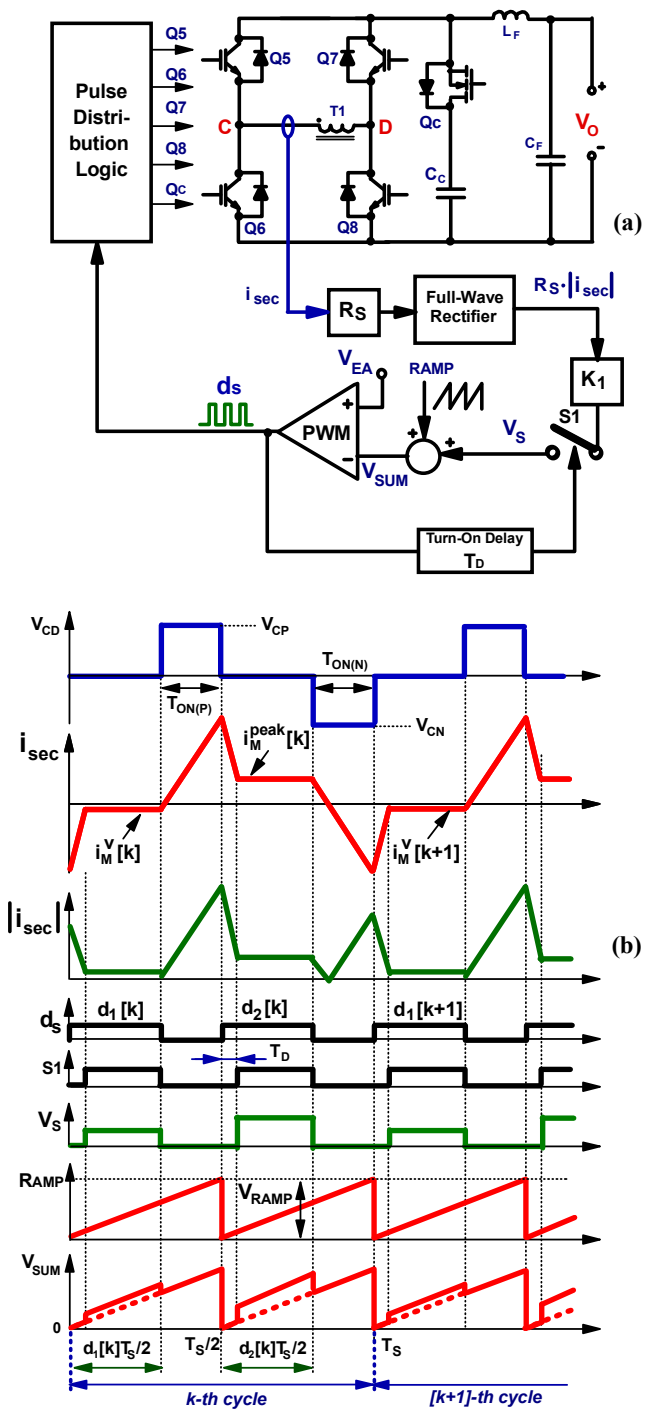

Fig. 5. Flux-balancing control for FB converter: (a) block diagram and (b) key waveforms.

does not affect converter operating point, i.e., average duty cycle D of the PWM output signal is not changed, namely

$$D = (d_1[k] + d_2[k])/2 \ , \tag{12}$$

With these assumptions, the following equations can be written for the first half of k-th cycle

$$d_1[k] \cdot V_{RAMP} - K_P \cdot i_M^V[k] = V_{EA}, \tag{13}$$

$$i_M^{peak}[k] = i_M^v[k] + V_{CP} \cdot (1 - d_1[k]) \cdot T_S/(2L_M) \tag{14}$$

and for the second half of k-th cycle

$$d_2[k] \cdot V_{RAMP} + K_P \cdot i_M^{peak}[k] = V_{EA}, \tag{15}$$

$$i_M^v[k+1] = i_M^{peak}[k] - V_{CN} \cdot (1 - d_2[k] - \Delta d) \cdot T_S/(2L_M), \tag{16}$$

where $K_P = R_S \cdot K_1$.

From linear Eqs. (12)-(16), the difference equation for valley current i_M^v is obtained as

$$i_M^v[k+1] = i_M^v[k] \cdot C_1 + C_0 \ , \tag{17}$$

where

$$C_1 = \left(1 - \frac{K_P \cdot T_S \cdot V_{CP}}{2 \cdot V_{RAMP} \cdot L_M}\right) \cdot \left(1 - \frac{K_P \cdot T_S \cdot V_{CN}}{2 \cdot V_{RAMP} \cdot L_M}\right), \tag{18}$$

$$C_0 = (V_{CP} - V_{CN}) \cdot (1 - V_{EA}/V_{RAMP}) \cdot T_S/(2 \cdot L_M) + \frac{T_S \cdot V_{CN} \cdot \Delta d}{2 \cdot L_M} - \frac{K_P \cdot (T_S/L_M)^2 V_{CP} \cdot V_{CN}}{4 \cdot V_{RAMP}} \cdot (1 - V_{EA}/V_{RAMP}), \tag{19}$$

$$V_{EA} = D \cdot V_{RAMP} + K_P \cdot V_C \cdot (1 - D) \cdot T_S/(4 \cdot L_M) \tag{20}$$

The discrete-time domain solution of difference Eq. (17) is

$$i_M^v[k] = i_M^v[0] \cdot C_1^k + C_0 \cdot \left(1 - C_1^k\right)/(1 - C_1). \tag{21}$$

In steady-state operation, $i_M^v[k+1] = i_M^v[k]$ and the steady-state value of magnetizing current is easily obtained from Eq. (17) as

$$i_M^v[k] = C_0/[1 - C_1]. \tag{22}$$

The dc magnetizing current during k-th switching period is defined as

$$i_M^{dc}[k] = \left(i_M^v[k] + i_M^{peak}[k]\right)/2, \tag{23}$$

The steady-state value of $i_M^{dc}[k]$ was computed from Eqs. (18)-(20) and (22)-(23). Calculated normalized steady-state dc current $i_M^{dc}[k]/i_{M\,max}^{dc}$ is plotted in Fig. 6 as a function of control gain K_P, where $i_{M\,max}^{dc}$ value, determined by Eq. (5), corresponds to the onset of transformer saturation. In Fig. 6, dc magnetizing current is shown for different values of duty cycle imbalance Δd. The graph in Fig. 6, as well as the graph in Fig. 7 were obtained for switching frequency f_S=30 kHz, clamp capacitor voltage V_C=430 V, duty cycle D = 0.5, magnetizing inductance L_M=4.1 mH, PWM ramp amplitude V_{RAMP}=2 V, transformer core cross-sectional area A_C=280 mm^2, saturation flux density B_{SAT}=0.37 T, and number of secondary winding turns N_S=48. Finally, the parameters that model transformer volt-second imbalance were V_{CP} = 431 V, V_{CN} = 429 V.

Dynamics of the flux-balancing loop are determined by the root of single-order characteristic polynomial **P(z),** which corresponds to difference Eq. (17). Namely,

$$P(z) = z - C_1 \tag{24}$$

Characteristic polynomial **P(z)** has single real root $z_1 = C_1$.

For stability analysis of the proposed control, it is assumed $V_{CP} = V_{CN} = V_C$, where V_C is the steady-state clamp capacitor voltage. Then, expression for root z_1 can be simplified as

$$z_1 = (F - 1)^2 \ , \tag{25}$$

where F is normalized control gain

$$F = \frac{K_P \cdot T_S \cdot V_C}{2 \cdot V_{RAMP} \cdot L_M} \ . \tag{26}$$

As z_1 value cannot be negative, the flux-balancing control transient response is always monotonic. The plot of root z_1 magnitude versus gain K_P is shown in Fig. 7. As can be seen in

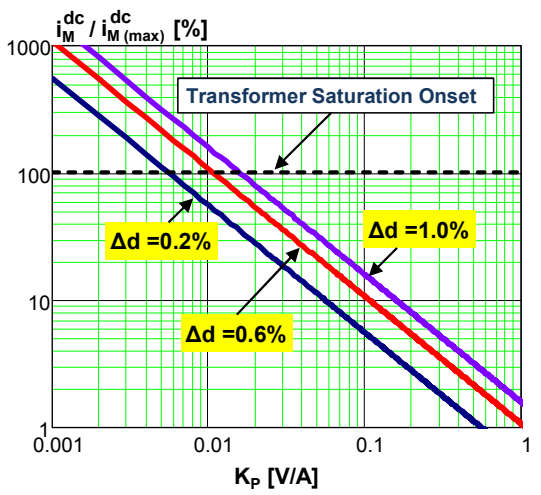

Fig. 6. Normalized steady-state dc magnetizing current versus gain K_p for flux-balancing control of FB converter.

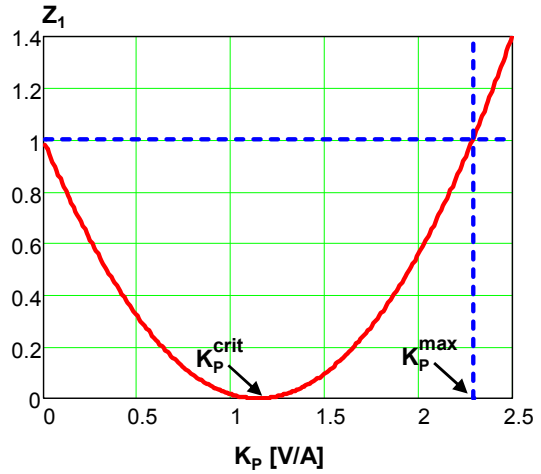

Fig. 7. Characteristic polynomial root value versus gain K_P for flux-balancing control of FB converter.

Fig. 7, at low K_P values, increase of gain K_P causes magnitude of root z_1 decrease until it reaches zero at

$$K_P^{crit} = \frac{2 \cdot V_{RAMP} \cdot L_M}{T_S \cdot V_C} \quad , \tag{27}$$

that corresponds to $F = 1$. As gain K_P increases further, the magnitude of root z_1 increases and reaches unity at K_P^{max}, which corresponds to $F = 2$. Increase of gain K_P above K_P^{max} makes the loop unstable. From Eq. (26), K_P^{max} value is given by

$$K_P^{max} = \frac{4 \cdot V_{RAMP} \cdot L_M}{T_S \cdot V_C} \quad . \tag{28}$$

It should be noted that the fastest transient response occurs when z_1 is minimal, i.e., for critical gain K_P^{crit}.

(B) Design Guidelines

The key design parameter for flux-balancing control is gain K_P, whose choice must meet the required level of dc magnetizing current and provide fast transient response while keeping the control loop stable. To prevent transformer saturation, the flux-balancing control must keep the dc magnetizing current well below $i_{M\,(max)}^{dc}$, determined by Eq. (5). It is important to consider the worst-case operating point and parameter values for calculation $i_{M\,(max)}^{dc}$ from Eq. (5). Once the desired maximum level of dc magnetizing current is selected, minimum gain value K_P^{min} can be found from Fig. 6. For example, to limit the dc magnetizing current to below 5% of the saturation level, assuming that the worst-case duty ratio imbalance is $\Delta d = 1\%$, gain K_P must be larger than approximately 0.32 V/A, i.e., $K_P^{min} > 0.32$ V/A.

The dynamic performance of flux-balancing control is also important because this control should be much faster with respect to output voltage / current control to avoid interaction between the two loops and maintain flux balancing during source-voltage and/or load-current transients. Since the fastest transient response is obtained for $K_P = K_P^{crit}$, the design goal is to select gain to be equal or close to K_P^{crit}. Therefore, if $K_P^{min} < K_P^{crit}$, then $K_P = K_P^{crit}$ is the best design choice. Otherwise, $K_P = K_P^{min} < K_P^{max}$ is the most prudent choice. For the example given above, since $K_P^{min} \cong 0.32$ is lower than $K_P^{crit} \cong 1.14$, selecting gain $K_P = K_P^{crit} = 1.14$ V/A is the optimal choice.

(C) Experimental Results

The proposed control was implemented in a 2-kW bidirectional FB converter prototype designed for automotive charging applications with the following input / output specifications and key component values:

- input voltage V_{IN} = 390 V;
- battery voltage range V_{BAT} = 240-360 V;
- switching frequency f_S = 30 kHz;
- transformer turns ratio N = 48:48;
- transformer leakage inductance L_{LEAK} = 2.4µH;
- resonant inductor value L_R = 16 µH;
- output inductor value L_F = 400 µH;
- active clamp capacitor C_C = 2.2 µF.

Measured key waveforms of the experimental converter operating in the battery discharging mode (boost mode) are shown in Fig. 8. As can be seen in Fig. 8(a), without the flux-balancing control the secondary current exhibits a significant difference between the positive and negative magnetizing-current levels that are shown inside the red circles, indicating the existence of the relatively high dc component of the magnetizing current. The same waveform with flux-balancing control shows a very well balanced magnetizing current, as can be seen in Fig. 8(b). Also observation of V_{SUM} waveform in Fig. 8(b) demonstrates addition of the current-balancing signal to the PWM ramp, shown inside blue rectangles.

The converter was tested in the entire range of battery voltage and discharging current without any signs of transformer saturation.

IV. Flux-Balancing Control of DAB Converter

Key waveforms of the DAB converter for the power transfer from source V_{IN} to V_O are shown in Fig. 9. The most important difference between the bidirectional FB converter waveforms in Fig. 4 and the DAB converter waveforms in Fig. 9 is that the primary current in the DAB converter is continuous, i.e., it does not have time intervals where it is zero as in the case of the primary current in the FB converter. As a result, the magnetizing current value cannot be extracted by sensing only the primary or the secondary current. In fact, in the DAB converter both primary

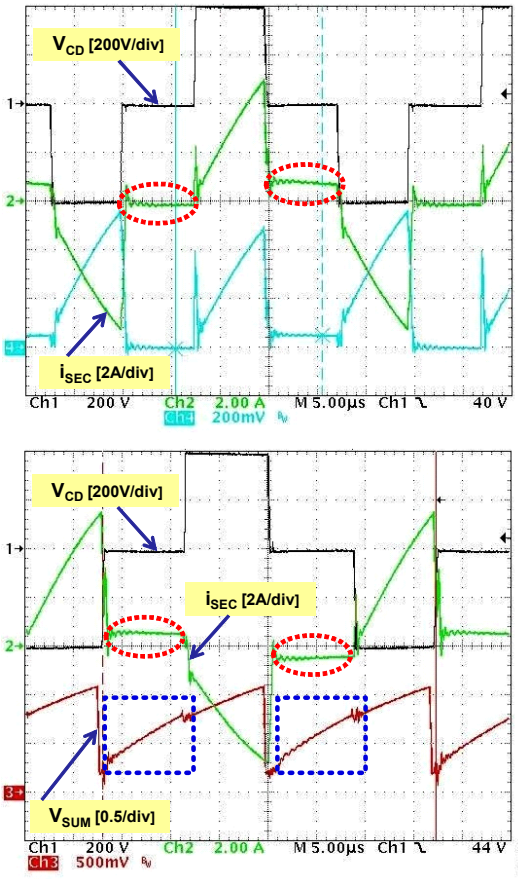

Fig. 8. Measured waveforms of FB converter operating (a) without flux-balancing control and (b) with flux-balancing control.

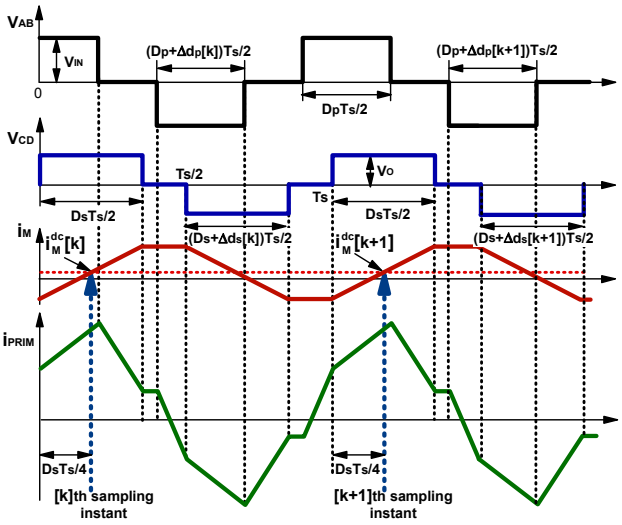

Fig. 9. Key waveforms of DAB converter.

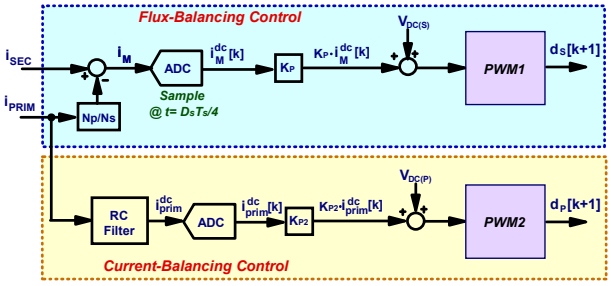

Fig. 10. Functional diagram of proposed flux-balancing and current-balancing controls for DAB converter.

and secondary currents must be sensed to be able to calculate the magnetizing current using Eq. (2).

The block diagram of a digital implementation of the proposed flux-balancing control is shown in the upper half of Fig. 10. In this control, in the k-th switching cycle magnetizing current i_M is sampled by the A/D converter at time instant $D_S \cdot T_S/4$ to determine its dc value $i_M^{dc}[k]$. The flux-balancing loop then computes flux-balancing control signal $K_P \cdot i_M^{dc}[k]$ that is summed with constant signal $V_{DC(S)}$ and applied to the input of the PWM block to generate duty ratio $d_S[k+1] = D_S + \Delta d_S[k+1]$ of secondary switches Q5-Q8. It should be noted that duty ratio $d_S[k+1] = D_S + \Delta d_S[k+1]$ is applied to negative secondary voltage V_{CD} during [k+1]-th switching cycle to provide flux balancing. Constant signal $V_{DC(S)}$ is used to set the dc value of the secondary-side duty ratio D_S.

While the proposed flux-balancing control is effective in eliminating the dc component of the magnetizing current, it is not optimal. Namely, according to Eq. (2), the zero value of the average magnetizing current can be achieved with non-zero values of the average primary and secondary currents. This is not desirable because dc components of the primary and secondary currents increase component losses. To facilitate a better understanding of the problem, Fig. 11 shows the transformer current waveforms obtained by Simplis simulations of a DAB converter with and without flux-balancing control. In the simulation circuit, a flux imbalance is introduced by assuming that switches Q1, Q2, Q5, and Q6 have 150-mΩ on-state resistance, whereas switches Q1, Q2, Q5, and Q6 have 200-mΩ on-resistance, as well as that the duty cycles of the positive and negative voltage V_{AB} pulses are mismatched by 0.5 %. The operating conditions and key component values of the simulated DAB power stage are: input voltage V_{IN}= 390 V, output voltage V_O=340 V, output power P_O=3.3 kW, switching frequency f_S=35 kHz, turns ratio of transformer N=34:30, secondary-side magnetizing inductance L_M=3mH, primary-side leakage inductance L_S=3.2 µH, and primary inductance L_{AC}=80 µH.

As shown in Fig. 11(a), without the flux-balancing control, the dc magnetizing current is -1.69 A, which in most practical cases is high enough to saturate the transformer. With the flux-balancing control, as shown in Fig. 11(b), the magnitude of the dc magnetizing current is reduced to -12 mA, i.e., it is practically zero. However, as it can be seen from Fig. 11(b), the reduction of the dc component of the magnetizing current is achieved at the expense of a significantly increased secondary current. Specifically, with the flux-balancing control the dc component of the secondary current is -1.66 A which is much higher than 51 mA without the control. In this example, the increase of the dc

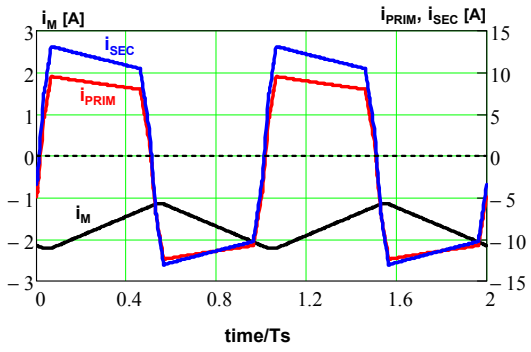

Current	i_M	i_{PRIM}	i_{SEC}
Dc Value	-1.69A	-1.43A	51mA

(a)

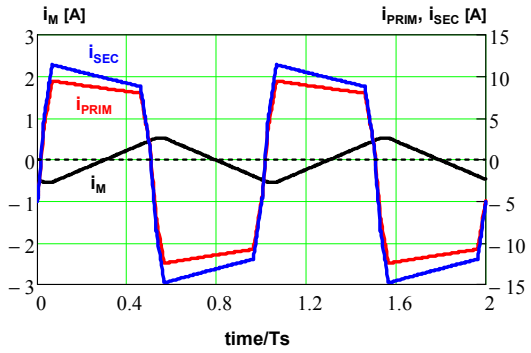

Current	i_M	i_{PRIM}	i_{SEC}
Dc Value	-12mA	-1.46A	-1.66A

(b)

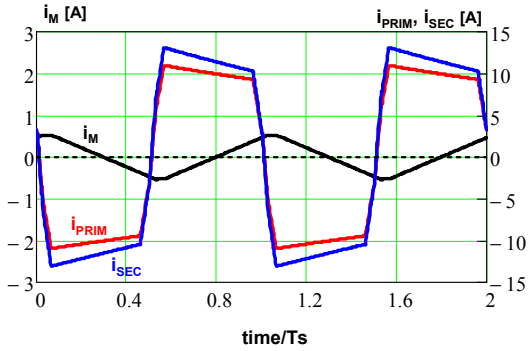

Current	i_M	i_{PRIM}	i_{SEC}
Dc Value	-0.4mA	-25mA	-28mA

(c)

Fig. 12. Simulated transformer current waveforms of DAB converter (a) without flux-balancing control, (b) with flux-balancing control only, and (c) with flux-balancing and current balancing controls.

component of the primary current due to the flux-balancing control is negligible since it changes from -1.43 A to -1.46 A.

To reduce the dc component of primary and secondary currents to a reasonable level, the second control loop is proposed, as shown in the lower half of Fig. 10. In the implementation in Fig. 10, the current-balancing loop uses the dc value of the sensed primary current obtained by low-pass (RC) filtering to adjust primary-side duty ratio $\boldsymbol{d_P}\,[\boldsymbol{k}] = \boldsymbol{D_P} + \Delta\boldsymbol{d_P}\,[\boldsymbol{k}]$ of negative primary voltage $\boldsymbol{V_{AB}}$ on a cycle-by-cycle basis. The primary-side duty ratio is obtained by sampling the output voltage of the analog RC filter that is proportional to $\boldsymbol{i_{PRIM}^{dc}}$ and computing current-balancing control signal $\boldsymbol{K_{P2}} \cdot \boldsymbol{i_{PRIM}^{dc}}\,[\boldsymbol{k}]$. The computed control signal is then summed with constant signal $\mathbf{V_{DC(P)}}$ and applied to the input of the PWM block to generate duty ratio of the primary switches Q1-Q4. Level of signal $\mathbf{V_{DC(P)}}$ determines the dc value of primary-side duty cycle $\boldsymbol{D_P}$.

As shown in Fig. 11(c), with the current-balancing loop, the dc components of the primary and secondary current are greatly reduced. Namely, with respect to the converter operation with only flux-balancing loop, the dc levels of the primary and secondary current are reduced from -1.46 A to -25 mA and from -1.66 A to -28 mA, respectively.

V. Summary and Future Work

Flux-balancing control for FB and DAB bidirectional dc-dc converters, based on sensing of the transformer magnetizing current, was presented. It was shown that in the FB converter in the boost operation mode the peak and valley values of the magnetizing current can be extracted from sensing single current waveform. However, in the DAB converter extraction of the magnetizing current waveform requires sensing of both primary and secondary currents. In the DAB converter, single-loop control of the magnetizing current can lead to excessive dc values of the winding currents. To avoid this issue, the current-balancing control loop was added which maintains the dc values of the transformer currents close to zero. For the FB converter, the discrete-time model was developed to analyze control steady-state accuracy, stability, and transient response and to provide design guidelines. Presented experimental results verify performance of the proposed flux-balancing control for the FB converter. The future work is experimental verification of the proposed two-loop control for the DAB converter, as well as its modeling and design-oriented analysis.

References

[1] N. Tan, T. Abe, and H. Akagi, "Topology and Application of Bidirectional Dc-Dc Converters," *Proc. IEEE Conference on Power Electronics- ECCE Asia,* 2011, pp. 1039-1046.

[2] K. Wang, F.C. Lee, and J. Lai, "Operation Principles of Bi-Directional Full-Bridge Dc/Dc Converter with Unified Soft-Switching Scheme and Soft-Starting Capability" *Proc. IEEE Applied Power Electronics Conference (APEC),* 2000, vol. 1, pp. 111-118.

[3] M. Kheraluwala, R. Gascoigne, D. Divan, and E. D. Baumann, "Performance Characterization of a High-Power Dual Active Bridge Dc-to-Dc Converter," *IEEE Trans. Industry Applications,* vol. 28, no. 6, Nov./Dec.1992, pp. 1294-1301.

[4] L. Zhu, "A Novel Self-Commutating Isolated Boost Full-Bridge ZVS-PWM Dc-Dc Converter for Bidirectional High-Power Applications," *IEEE Trans. Power Electronics,* vol. 21, no. 2, Mar. 2006, pp. 422-429.

[5] H. Bai and C. Mi, "Eliminate Reactive Power and Increase System Efficiency of Isolated Bidirectional Dual-Active-Bridge Dc-Dc Converters

Using Novel Dual-Phase-Shift Control," *IEEE Trans. Power Electronics,* vol. 23, no. 6, Nov. 2008, pp. 2905-2914.

[6] H. Zhou and A. M. Khambadkone, "Hybrid Modulation for Dual-Active-Bridge Bidirectional Converter With Extended Power Range for Ultracapacitor Application," *IEEE Trans. Industry Applications,* vol. 45, no. 4, Jul./Aug. 2009, pp. 1434-1442.

[7] G. G. Oggier, G. O. García, and A. R. Oliva, "Modulation Strategy to Operate the Dual Active Bridge Dc-Dc Converter Under Soft Switching in the Whole Operating Range," *IEEE Trans. Power Electronics,* vol. 26, no. 4, Apr. 2011, pp. 1228-1236.

[8] A. K. Jain and R. Ayyanar, "PWM Control of Dual Active Bridge: Comprehensive Analysis and Experimental," *IEEE Trans. Power Electronics,* vol. 26, no. 4, Apr. 2011, pp. 1215-1227.

[9] F. Krismer and J.W. Kolar, "Efficiency-Optimized High-Current Dual Active Bridge Converter for Automotive Applications," *IEEE Trans. Industrial Electronics,* vol. 59, no. 7, Jul. 2012, pp. 2745-2760.

[10] N. Tan, T. Abe, and H. Akagi, "Design and Performance of a Bidirectional Isolated Dc-Dc Converter for a Battery Energy Storage System," *IEEE Trans. Power Electronics,* vol. 27, no. 3, Mar. 2012, pp. 1237-1248.

[11] D. Vinnikov, J. Laugis, and I. Galkin, "Middle-Frequency Isolation Transformer Design Issues for the High-Voltage Dc/Dc Converter," *Proc. IEEE Power Electronics Specialists Conference,* 2008, pp. 1930-1936.

[12] R. Naayagi, A. Forsyth, and R. Shuttleworth, "High-Power Bidirectional Dc-Dc Converter for Aerospace Applications," *IEEE Transactions on Power Electronics,* vol. 27, no. 11, November 2012, pp. 4366-4379.

[13] H. Weischedel, and G. Westerman, "A Symmetry Correcting Pulsewidth Modulator for Power Conditioning Applications," *IEEE Transactions on Industry Applications,* vol. IA-9, no. 3, May-June 1973, pp. 318-322.

[14] R. Redl, N. Sokal, and C. Shaefer, "Transformer Saturation and Unusual System Oscillation in Capacitively Coupled Half-Bridge or Full-Bridge Forward Converters: Causes, Analysis, and Cures," *Proc. IEEE Power Electronics Specialist Conference,* 1988, pp. 820-829.

[15] J. Claassens and I. Hofsajer, "A Flux Balancer for Phase-Shift ZVS Dc-Dc Converters Under Transient Conditions," *Proc. IEEE Applied Power Electronics Conference,* 2006, pp. 523-527.

[16] G. Kamath, "Simple Control Method Tames Flux Saturation in High-Frequency Transformer-Link Full-Bridge Dc-Dc Converters," *How2Power Today,* June 2012, pp. 1-6.